Technical Report

UDC 669 . 14 . 018 . 44 : 621 . 791 . 754 . 3 : 539 . 434 : 620 . 184 / . 186

Creep Rupture Strength and Microstructures of SAVE12AD Welded Joints

Tomoaki HAMAGUCHI* Hirokazu OKADA
Hiroyuki HIRATA Shinnosuke KURIHARA
Hiroyuki SEMBA Mitsuru YOSHIZAWA

Abstract

The new ferritic heat-resistant steel SAVE12AD has been developed for large diameter and heavy wall thickness pipes and forgings of fossil-fired power boilers. The long-term creep rupture strength of welded joints showed smaller degradation than that of conventional ferritic steels. No fine grain area was observed in the microstructure after the simulating weld heat-affected zone at just above A_{C3} transformation temperature, although there were fine grains along prior austenite grain boundaries.

1. Introduction

Fossil-fired power plant boilers are now required to operate at higher temperature and pressure to enhance power generation efficiency and thereby reduce CO_2 emission.[1] In appreciation of the lower linear expansion coefficient and more economical price than those of conventional austenitic steels and Ni alloys, high-Cr ferritic heat-resistant steel typically such as ASME Gr. 91 and 92 is now used widely for heavy-diameter and large-wall thickness steam pipes for the boilers of such power plants. SAVE12AD, developed by Nippon Steel & Sumitomo Metal Corporation, has higher creep rupture strength both in the base metal and welded joints than the conventional steels used for this application, and as such, its application as a new heat-resistant material is expected to expand to effectively improve power generation efficiency.[2]

Table 1 shows the alloy design concept of SAVE12AD. It was designed as an improvement on 11Cr ferritic heat-resistant steel, SAVE12 (0.1C-11Cr-3W-3Co-V-Nb-Ta-Nd-N, in mass%).[3] Co is added by 3 mass% to raise the strength of the martensite matrix and suppress the formation of δ ferrite,[3] W by 3 mass% for solid solution hardening and precipitation hardening by the Laves phase of Fe_2W, and Nd by 0.03 mass% to improve ductility to suppress creep rupture.[4] In addition, the content of Cr is set at 9 mass% in consideration of the following: that creep rupture strength is lowered when thermally unstable MX type carbo-nitrides slowly transform into the Z phase;[5] and that long-term creep rupture strength is markedly lowered during long use as a result of the coarsening of $M_{23}C_6$ particles, the increase in their inter-particle distance, the disappearance of dislocations and the consequent recovery of lath martensite.[6–9] B is added by 0.01 mass% because it prevents $M_{23}C_6$ precipitating at grain boundaries from coarsening and, by thus suppressing the disappearance of dislocations in the lath martensite, serves to maintain long-term creep rupture strength.[10–12]

With respect to welded joints, on the other hand, significant degradation of the mean creep rupture strength of welded joints below that of the base metal has been viewed as a serious problem with conventional high-Cr ferritic heat-resistant steels.[13] The failure type in such weakened welded joints is type IV taking place at the portions of fine-grain structure in the heat-affected zones (HAZs). There have been various suggestions as to the cause of the type IV failure of these types of steel besides the fine structure: the suggested causes include insufficient quantity of precipitates at both prior austenite grain boundaries and the interfaces of martensite during post weld heat treatment (PWHT) applied to relax residual stress and creep deformation.[14, 15]

To suppress the type IV failure, B addition is considered effective at preventing fine structure from forming, because B segregates at martensite interfaces to lower interface energy and minimizes the diffusion type inverse austenitic transformation during welding.[12, 15, 16–18] To bring about these effects of B, it is necessary to control the precipitation of BN, which takes place thermally stably at high temperature, and for this purpose, the content of N is limited to 0.01 mass%.[19] Limiting the amount of N to 0.01 mass% is effective also for minimizing the decrease in MX precipitation hardening resulting from the formation of the Z phase. It is necessary to obtain

* Researcher, Pipe & Tube Research Lab., Steel Research Laboratories
1-8 Fuso-cho, Amagasaki City, Hyogo Pref. 660-0891

Table 1 Alloy design concept of SAVE12AD

Elements	Objectives	Improvements
9Cr	• Long-term creep strength	Creep strength of base metal
3W	• Laves phase precipitation strengthening • Solution strengthening	
0.01B	• Suppression of $M_{23}C_6$ coarsening on G.B.	
0.01N (low-N)	• Suppression of Z-phase • BN precipitation	
0.03Nd	Suppression of S segregation	Creep ductility
3Co	Stability of martensite	Toughness
0.01B	Suppression of fine grain in HAZ	Creep strength of welded joint

Table 2 Chemical compositions ranges of SAVE12AD (mass%)

C	Si	Mn	P	S	Cr	Ni	W	Co	V	Nb+Ta	Nd	B	Sol. Al	N	O
0.05/ 0.10	0.05/ 0.50	0.20/ 0.70	≤0.020	≤0.008	8.50/ 9.50	≤0.20	2.5/ 3.5	2.5/ 3.5	0.15/ 0.30	0.05/ 0.12	0.010/ 0.060	0.007/ 0.015	≤0.030	0.005/ 0.015	≤0.0050

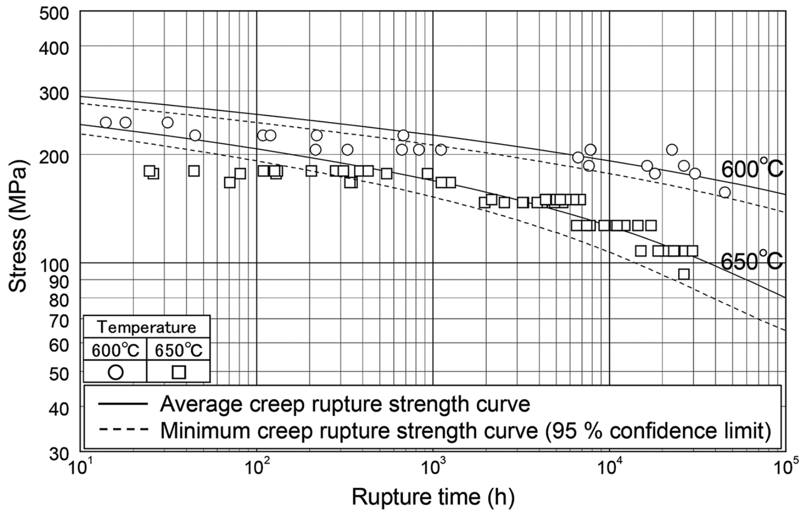

Fig. 1 Creep rupture strength of SAVE12AD base metal

good weldability as well as high creep rupture strength of both the base metal and welded joints, excessive addition of B lowers weldability, and in consideration of these, the target addition amount of B is set at 0.01 mass%.

Based on the above alloy design philosophy, the chemical composition of SAVE12AD is set as given in **Table 2**. The results of creep rupture test at 600 and 650°C using test pieces of large- and small-diameter pipes and flat plates of the steel prepared according to the chemical composition ranges in Table 2 are shown in **Fig. 1**. The graph also shows the average creep rupture strength curves (in solid lines) and their 95% confidence limit (in dotted lines) at both the test temperatures; these were obtained by regression of the rupture test data by the Larson-Miller method. Note that, for high regression accuracy in the long-term zone, the results only of the specimens that failed after 500 h or more had elapsed were used for the regression. SAVE12AD has been included in the standard of the American Society of Mechanical Engineers (ASME) as Code Case 2839; the allowable stress of its base metal at 600°C is rated at 1.5 times that of Gr. 91, and 1.2 times that of Gr. 92, approximately.

The present paper explains the long-term creep rupture characteristics and the metallographic structure of welded joints of SAVE 12AD.

2. Specimens and Experimental Procedure

Welded joint tubes, 38.1 mm in outer diameter and 8.8 mm in wall thickness, were prepared by automatic gas tungsten arc welding with commercial filler wire AWS A5.28 ER90S-G and A5.14 ERNiCr-3, and then applying PWHT at 740°C for 30 min (see **Tables 3 and 4** and **Fig. 2**). Creep rupture test pieces, each having a parallel portion 6 mm in diameter and 30 mm in length, were cut out from the welded joint tubes thus prepared in such a way that the weld line came at the center of the parallel portion. The creep tests were conducted at 600 and 650°C applying stress of 78.5 to 215.7 MPa. After the test, the metallographic structures of the test pieces were observed through an optical microscope and a transmission electron microscope (TEM).

To evaluate the metallographic structure of HAZs independently from the effects of different welding methods and conditions, bar test pieces, 7 mm in diameter and 12 mm in length, were cut out from tubes, 45 mm in outer diameter and 8.5 mm in wall thickness;

Table 3 Chemical compositions of weld metals (mass%)

Weld metal	C	Si	Mn	P	S	Co	Ni	Cr	Mo	W	V	Nb	Ti	N
ER90S-G	0.07	0.31	0.78	0.003	0.003	0.98	0.46	10.04	0.34	1.46	0.21	0.036	—	0.04
ERNiCr-3	0.03	0.19	2.99	0.003	0.002	—	75.00	18.40	—	—	—	2.70	0.39	—

Table 4 Welding conditions

Welding process	Automatic GTAW
Pass sequences	1–8
Current (A)	100–130
Voltage (V)	13–14
Traveling speed (mm/s)	1.67
Heat input (kJ/mm)	0.8–1.1
Shielding gas	Pure Ar
Preheating	N/A
PWHT	740°C for 30 min

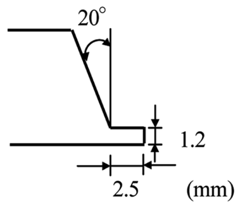

Fig. 2 Bevel configuration of welded joint

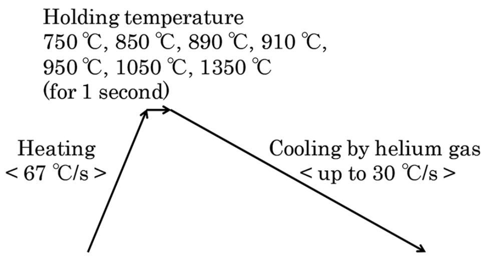

Fig. 3 Simulated welding heat cycle

here, the A_{C1} and A_{C3} transformation temperatures of the steel were 800 and 896°C, respectively. The test pieces were subjected to simulated welding heat cycles using a Formaster Press made by Fuji Electronic Industrial Co., Ltd., whereby they were heated and held at 750, 850, 890, 910, 950, 1 050 and 1 350°C for 1 s, and then rapidly cooled by blowing helium gas; **Figure 3** shows the simulated heat cycle. After the test, the metallographic structure of the test pieces was observed by the "scanning electron microscope-electron back scatter diffraction patterns" (SEM-EBSD) method.

3. Test Results and Discussion

3.1 Creep rupture strength of SAVE12AD welded joints

Figure 4 shows the results of the creep rupture tests of SAVE 12AD welded joints together with those of the base metal; WM, BM, FL and HAZ in the graph indicate that the specimens ruptured at the weld metal, the base metal, the fusion line and the HAZ, respectively. All the welded specimens that ruptured before 20 000 h had elapsed withstood longer than the minimum rupture strength of the base metal, and there was no significant difference in the creep rupture strength between the two weld metals. The ruptured position, in contrast, was different depending on the weld metal: with ER90S-G, either type I failure occurred at the weld metal or type II at the position from the weld metal to the HAZ, and with ERNiCr-3, the fracture occurred at either the base metal or the fusion line.

The difference of the ruptured position between the two weld metals is presumably due to the difference in the creep rupture strength between the SAVE12AD base metal and the weld metals: since the creep rupture strength of ER90S-G is lower than that of SAVE12AD, the fracture occurred at the weld metal, and on the other hand, the creep rupture strength of ERNiCr-3 is higher, and consequently the specimens ruptured at the base metal or near the fusion line. At the low-stress creep tests exceeding 20 000 h, in contrast, the creep rupture of all the specimens was below the minimum

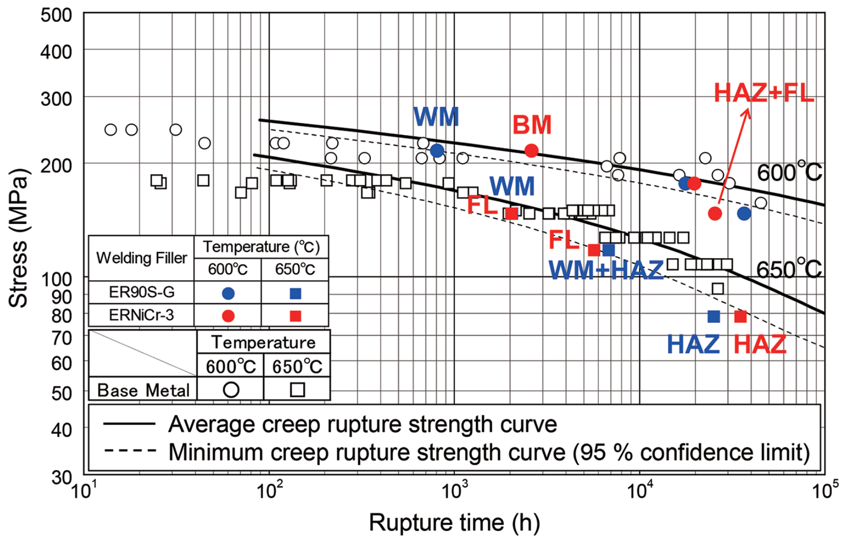

Fig. 4 Creep rupture strength of SAVE12AD base metal and welded joints

rupture strength curves of the base metal, meaning shorter creep rupture occurs, regardless of the type of weld metal. At either test temperature, there was no marked difference in the creep rupture strength between the two weld metals, and the fracture occurred at or near the HAZ.

With conventional steels, Gr. 92 for instance, the creep rupture strength of welded joints decreases to below that of the base metal after roughly 10 000 h of use at 600°C or after roughly 1 000 h at 650°C.[13] According to the result of the present test, however, while the creep rupture strength of SAVE12AD welded joints became lower than that of the base metal at the low-stress level, it began to decrease after elapsing for a longer time than in the cases of conventional steels. In addition, the degradation of the creep rupture strength of welded joints against that of the base metal of SAVE 12AD was smaller than the same of conventional steels.

3.2 Metallographic structure of SAVE12AD welded joints after creep rupture

The previous sub-section 3.1 stated that the degradation of the creep rupture strength of welded joints was smaller with SAVE 12AD than with conventional steels. In relation to this, observation results of the metallographic structure of a welded joint after the rupture test are explained below.

The observation object is the specimen that ruptured after 25 582 h of creep rupture test at 600°C under a stress of 147 MPa. Optical micrographs of the fracture surface in the parallel portion are given in parts (a) to (e) of **Fig. 5**. The fracture ran obliquely from the HAZ on the outer-surface side of the tube to the fusion line on the inner-surface side. To examine the metallographic structure of the HAZ in detail, the structure of the parallel portion was observed from the fracture side to the other side across the weld metal. While no defects such as voids or cracks were found near the fusion line, a series of voids, tens of micrometers in size, were found to align in the HAZ nearly in parallel to the fusion line about 1 mm away from it. Typical lath martensite was found in a field of view roughly 5 mm from the fusion line, where the structure was presumed to be substantially the same as that of the base metal.

To study the structure in more detail, a thin-film specimen was extracted from the base metal in the parallel portion of the test piece, and its structure was observed through a TEM; bright-field images thus obtained are given in **Fig. 6**. Lath martensite was confirmed to survive also in the base metal like in the structure of the base metal after a long-term creep rupture test.[20] In addition $M_{23}C_6$ was ob-

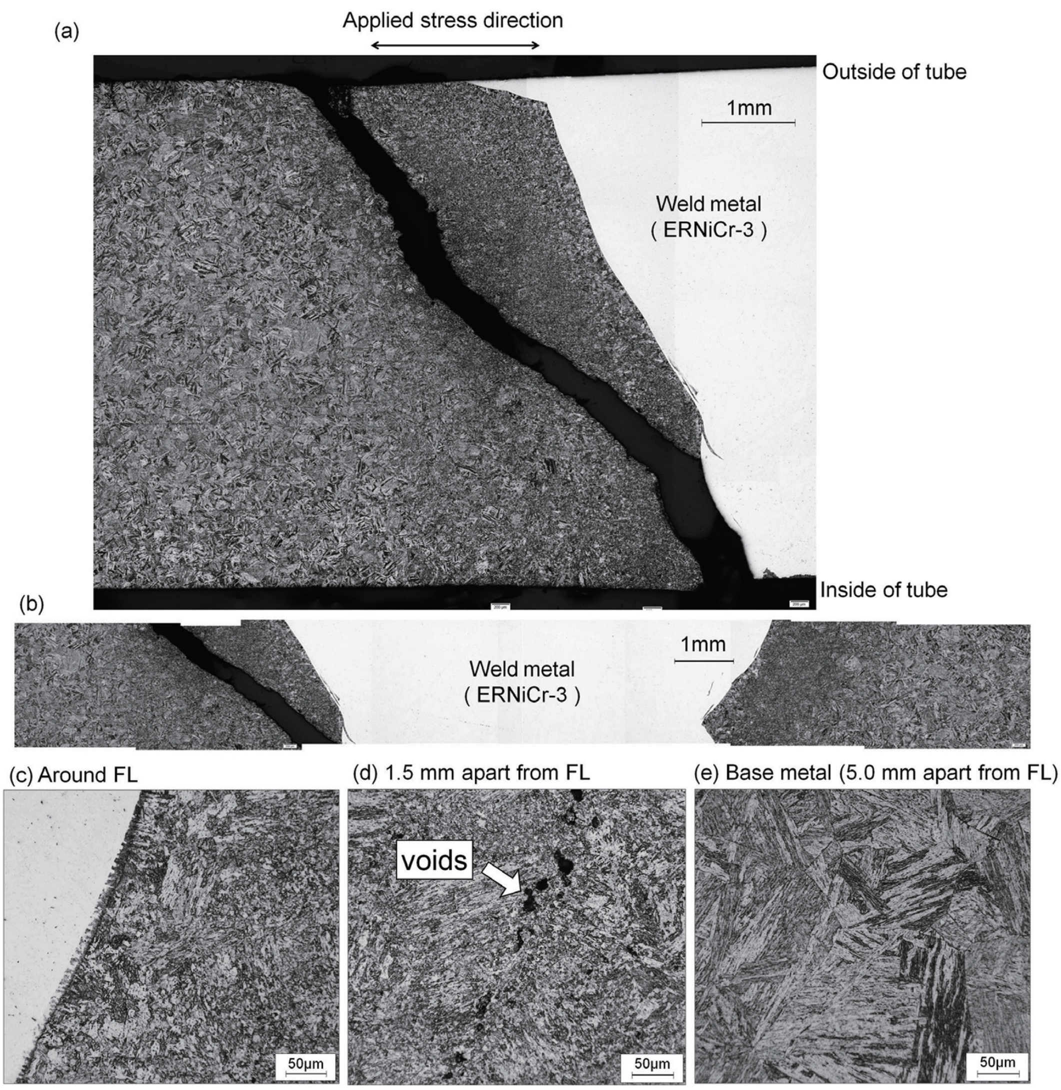

Fig. 5 Optical micrographs of SAVE12AD welded joint after creep testing

served in particles 80 nm or so in size at prior austenite grain boundaries and the interfaces of laths and blocks, but marked coarsening of $M_{23}C_6$ as seen in conventional steels[7–9] was not found in spite of the long-term creep deformation for more than 25 000 h.

Then, to confirm the metallographic structure of the HAZ, we cut out a thin-film specimen from a part of the HAZ about 1 mm from the fusion line, and observed its structure through a TEM. **Figure 7** shows its TEM micrographs and the element analysis charts of precipitates obtained by energy dispersive X-ray spectrometry (EDS). Different from the base metal, where lath martensite structure was maintained through the test, greatly recovered and recrystallized equiaxed grains were found in the specimen. From the precipitation analysis results by EDS, the intra-granular precipitates, 100 nm or so in size, at Points 1 to 3 were identified as $M_{23}C_6$, and the precipitates, hundreds of nanometers in size, at the interfaces at Points 4 and 5 as the Laves phase. Since MX was confirmed to exist in tempered specimens,[20] it had been presumed to survive creep deformation before the test, but it was not found in the present exami-

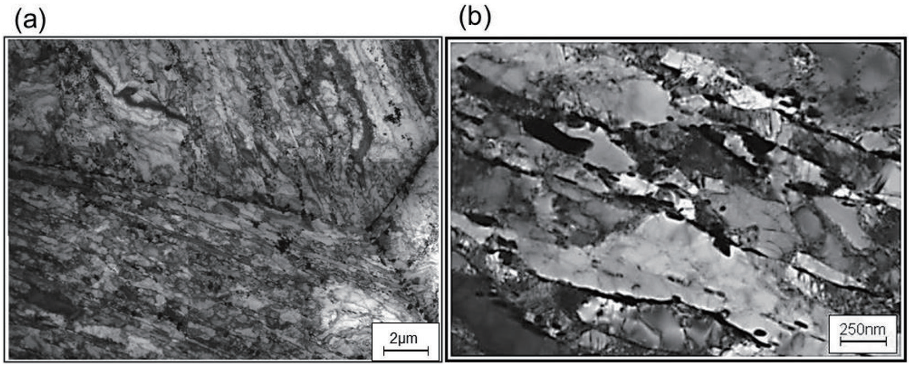

Fig. 6 TEM micrographs of base metal of SAVE12AD welded joint after creep testing

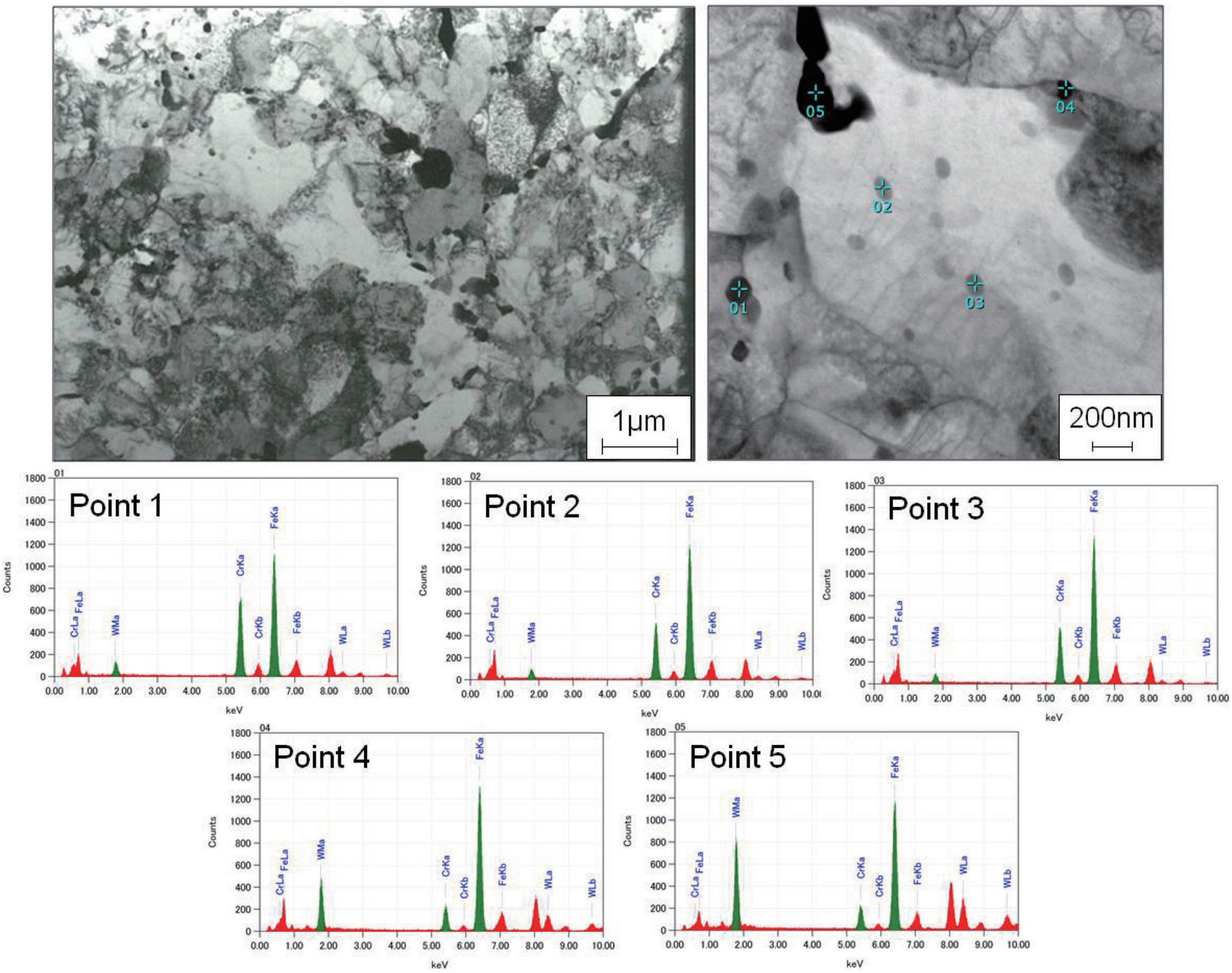

Fig. 7 TEM micrographs and EDS analysis results of HAZ of SAVE12AD welded joint after creep testing

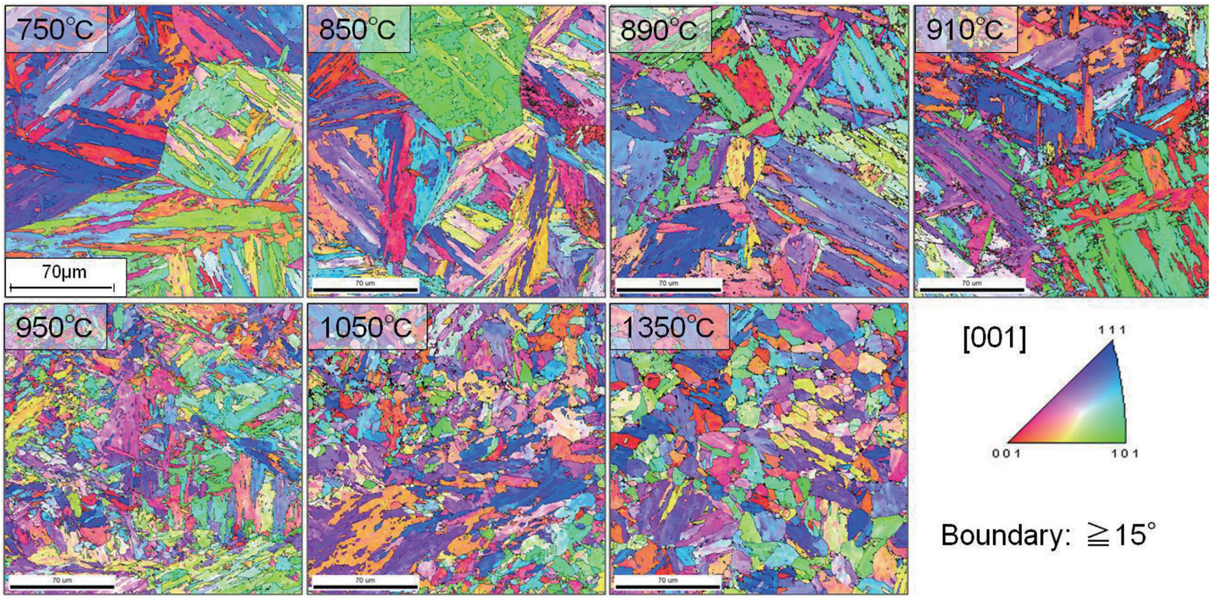

Fig. 8 Orientation maps of microstructures after welding heat cycle simulation

nation.

As has been explained above, although significant coarsening of precipitates was not seen in the HAZ portion roughly 1 mm from the fusion line, sub-grain structures were prominent, which seemed to indicate that the HAZ was the weakest part of SAVE12AD welded joints in terms of creep strength.

3.3 Metallographic structure after welding heat cycle simulation test

In the previous sub-section 3.2, the HAZ portion roughly 1 mm from the fusion line was presumed to be the weakest part of welded joints of SAVE12AD in terms of creep rupture strength. Presented below is the result of detailed observation of the metallographic structure of the HAZ of the steel after the welding heat cycle simulation test.

Figure 8 shows the orientation maps after the welding heat cycle simulation test at different maximum temperatures. In the case where the maximum temperature was 750°C, lower than the A_{C1} transformation temperature, a typical lath martensite structure was observed. In the case of 850°C, between the A_{C1} and the A_{C3} transformation temperatures, lath martensite nearly the same as in the above case was observed. After the heat cycle to 890°C, in the dual-phase range near the A_{C3} transformation temperature, although the structure consisted mainly of lath martensite, the formation of grains 1 μm or so in size were found at prior austenite grain boundaries and the interfaces of intra-grain blocks and packets. When the maximum temperature was 910°C, slightly over the A_{C3} transformation point, where fine-grain structure is dominantly seen with conventional steels, grains 1 μm or so in size were confirmed at most prior austenite grain boundaries, but the fine-grain structure seen with conventional steels[21–23] was not found. In the cases of 950 and 1 050°C, fine grains at the interfaces coarsened as the temperature rose, and the metallographic structure observed was a mixture of these comparatively coarse grains and fine grains. In the case of 1 350°C, the structure consisted of prior austenite grains 30 to 70 μm in size.

The result of this welding heat cycle simulation test made it clear that the formation of the fine-grain structure, which takes place in the case of conventional steels at slightly above the A_{C3} transformation temperature, was suppressed with SAVE12AD. In the heating temperature range from 950 to 1 050°C, on the other hand, two types of grains became manifest: one is those originating from prior austenite grain boundaries and the interfaces of laths and blocks, and the other is comparatively fine grains, which presumably formed through shear type inverse transformation and recrystallization. In this relation, there is a report to the effect that, when tempering, water cooling, sub-zero treatment, a welding heat cycle, and then PWHT are sequentially applied to Gr. 92 steel so that the size of prior austenite grains becomes 10 μm or so and precipitates form at grain boundaries and martensite interfaces, the relative decrease in the creep rupture strength of welded joints below that of the base metal is very small.[18] This indicates that the main cause of type IV fracture is not the fine-grain structure but the absence of precipitates at those interfaces. In the case of SAVE12AD, when it is heated to around 1 000°C, fine grains become manifest, but on the other hand, more precipitates form at the interfaces during PWHT and creep deformation than in the temperature range around 900°C, which probably led to the smaller decrease in the creep rupture strength of welded joints below that of the base metal than in the case of conventional steels. It is presumed that, at 1 350°C, although the prior austenite grains of the HAZ are finer than in the base metal owing to the austenitic inverse transformation and the formation of delta-ferrite, most of the precipitates that formed during the tempering heat treatment become solute again in the parent phase during the welding heat cycle, and precipitate at the interfaces during PWHT and creep deformation, bringing about precipitation hardening, and for this reason, there is a negligible decrease in the HAZ strength.

4. Conclusion

The examination results of the creep rupture strength and the metallographic structure of the welded joints of SAVE12AD, a new steel material expected to be useful for the boilers for next-generation thermal power plants, have been presented herein.

We clarified that, although the creep rupture strength of welded joints of SAVE12AD falls to below the average creep rupture strength of the base metal especially at the test at high temperature under low stress, the degree of the fall is smaller than that with conventional steels. This is presumably because the formation of fine-grain structure in the HAZ, which is the cause of the strength decrease of welded joints of conventional steels, is minimized in the case of SAVE12AD.

References

1) Ministry of Economy, Trade and Industry: Ref. for Tech. Roadmap for Next-generation Thermal Power Plants. Jul. 2015
2) Iseda, A. et al.: The Thermal and Nuclear Power Generation Convention Collected Works. 13, 35 (2017)
3) Igarashi, M., Sawaragi, Y.: International Conference on Power Engineering-97. 2, 107 (1997)
4) Yoshida, M. et al.: CAMP-ISIJ. 27, 1558 (2003)
5) Yoshizawa, M. et al.: Materials Science and Engineering A. 510–511, 162 (2009)
6) Hashizume, R. et al.: Tetsu-to-Hagané. 88 (11), 793 (2002)
7) Hassan Ghassemi Armaki, et al.: Materials Science and Engineering A. 527, 6581 (2010)
8) Hassan Ghassemi Armaki, et al.: Metallurgical and Materials Transaction A. 42A, 3084 (2011)
9) Hassan Ghassemi Armaki, et al.: Materials Science and Engineering A. 532, 373 (2012)
10) Takahashi, N. et al.: Tetsu-to-Hagané. 61 (9), 2263 (1975)
11) Horiuchi, T. et al.: ISIJ International. 42, S67 (2002)
12) Abe, F.: Bulletin of the Iron and Steel Institute of Japan. 17 (8), 560 (2012)
13) Yaguchi, M. et al.: PVP2012-78393. 2012
14) Liu, Y. et al.: Metallurgical and Materials Transaction A. 44A, 4626 (2013)
15) Abe, F. et al.: Material Science & Technology. 84 (6), 465 (2014)
16) Abe, F. et al.: Materials at High Temperatures. 23 (3–4), (2006)
17) Shirane, T. et al.: Science and Technology of Welding and Joining. 4 (8), 698 (2009)
18) Liu, Y. et al.: Metallurgical and Materials Transaction A. 45A, 1306 (2014)
19) Semba, H., Abe, F.: Energy Materials. 1 (4), 238 (2006)
20) Hamaguchi, T. et al.: 41st MPA–Seminar Proceeding.
21) Matsui, M. et al.: ISIJ International. 41, S126 (2001)
22) Hasegawa, Y. et al.: Tetsu-to-Hagané. 90 (10), 609 (2004)
23) Sakthivel, T. et al.: Materials Science and Engineering A. 591, 111 (2014)


Tomoaki HAMAGUCHI
Researcher
Pipe & Tube Research Lab.
Steel Research Laboratories
1-8 Fuso-cho, Amagasaki City, Hyogo Pref. 660-0891


Shinnosuke KURIHARA
Researcher
Pipe & Tube Research Lab.
Steel Research Laboratories


Hirokazu OKADA
Senior Researcher, Ph. D.
Pipe & Tube Research Lab.
Steel Research Laboratories

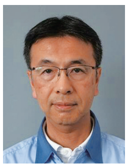
Hiroyuki SEMBA
Chief Researcher, Ph.D.
Pipe & Tube Research Lab.
Steel Research Laboratories


Hiroyuki HIRATA
General Manager, Head of Lab., Ph.D
Welding & Joining Research Lab.
Steel Research Laboratories


Mitsuru YOSHIZAWA
Senior Manager, Ph. D.
European Office